Vital Annex: International Journal of Novel Research in Advanced Sciences
ISSN: 2751-756X
Volume 04 Number 07 (2025)
https://innosci.org/IJNRAS

Article

Synthesis, *In Silico* Evaluation, and Biological Activity Assessment of Chalcone Derivatives Against MCF-7 Cells

Dhamer Ismael Madab[1]

1. Directorate of Education, Tikrit, Ministry of Education, Iraq.
* Correspondence: www.dhammer.84@gmail.com

Abstract: Chalcones, characterized by their distinct α,β-unsaturated carbonyl system, exhibit diverse therapeutic properties, including antimicrobial and anticancer activities. The current study focused on synthesizing novel chalcone derivatives using a base-catalyzed Claisen–Schmidt condensation reaction involving substituted benzaldehydes and acetophenone derivatives. These synthesized compounds were structurally verified using FTIR, ^{1}H NMR, and ^{13}C NMR spectroscopy, confirming the successful formation of chalcones via characteristic carbonyl and olefinic peaks. Biological evaluation included cytotoxic assays against the MCF-7 breast cancer cell line, using the MTT assay, where derivative 1C displayed significant cytotoxicity (approximately 10.93% cell viability at 320 ppm), markedly surpassing derivative 1A. Furthermore, antibacterial activities assessed through the agar diffusion method demonstrated pronounced inhibitory effects against Bacillus subtilis, Escherichia coli, and Streptococcus pneumoniae, with compound 1A exhibiting superior antibacterial activity. Additionally, molecular docking studies revealed that derivative 1C showed promising binding affinity (-7.69 kcal/mol) and favorable interactions with key amino acid residues within the estrogen receptor (PDB ID: 5T92), highlighting its potential mechanism of action. These findings emphasize the critical influence of structural variations on biological outcomes and suggest that further optimization of chalcone derivatives with different substitution patterns could yield potent, multifunctional therapeutic agents.

Keywords: Anticancer, Antibacterial, Chalcone, Claisen-Schmidt, MCF-7, Molecular docking.

Citation: Madab, D. I Synthesis, *In Silico* Evaluation, and Biological Activity Assessment of Chalcone Derivatives Against MCF-7 Cells. Vital Annex: International Journal of Novel Research in Advanced Sciences 2025, 4(7), 242-262

Received: 10th May 2025
Revised: 16th Jun 2025
Accepted: 24th Jul 2025
Published: 10th Aug 2025

1. Introduction

The persistent rise of bacterial resistance and breast cancer incidence poses significant challenges to modern medicine. Both health issues demand the development of innovative therapeutic strategies. While bacterial infections have been traditionally treatable with antibiotics, the emergence of multidrug-resistant (MDR) strains has drastically reduced treatment efficacy [1]. Currently, breast cancer continues to be the leading type of cancer in women worldwide, requiring the use of precise and efficient chemotherapeutic drugs. In both contexts, heterocyclic compounds have shown substantial promise due to their chemical diversity and biological activity [2].

Bacterial resistance has increasingly become a significant issue, largely return to the widespread misuse and overuse of antibiotics [3]. When antibiotics are improperly prescribed or utilized without appropriate medical supervision, they create selective pressure on microbial populations. As a result, resistant strains survive and multiply. Moreover, the horizontal transfer of resistance genes among bacteria has worsened the situation [4]. If current trends persist, many common infections could become untreatable. Therefore, it is crucial to discover new antimicrobial agents, particularly those with novel mechanisms of action. Heterocyclic compounds, which are organic molecules characterized by rings containing atoms such as nitrogen, oxygen, or sulfur, are promising

candidates due to their high binding affinity and adaptability to various molecular targets [5].

Simultaneously, breast cancer treatment faces similar challenges. Although traditional chemotherapy and hormone therapy have improved survival rates, their lack of selectivity often results in systemic toxicity and resistance. Recently, researchers have developed heterocyclic-based anticancer agents that can specifically target breast cancer cells, particularly those expressing estrogen receptors or exhibiting HER2 overexpression. These compounds can inhibit cell proliferation, induce apoptosis, and disrupt cancer metabolism [6]. For instance, several derivatives of thiazoles, pyrimidine, and quinoline have demonstrated cytotoxic effects against breast cancer cell lines while sparing normal tissues [7].

In addition, heterocyclic compounds provide a unique advantage in multifunctionality. If a single compound can exhibit both antimicrobial and anticancer properties, it may yield dual therapeutic benefits. This is especially relevant for immunocompromised cancer patients more susceptible to infections. The recent integration of heterocyclic scaffolds with nanotechnology has also improved drug delivery and bioavailability, thereby increasing therapeutic efficacy [8].

Chalcone derivatives, characterized by their α,β-unsaturated carbonyl system, play a vital role in medicinal chemistry due to their wide-ranging biological activities. Because of their conjugated structure, they interact effectively with various cellular targets, exhibiting anti-inflammatory, antimicrobial, and anticancer properties [9]. If appropriately substituted, chalcones can enhance selectivity and potency against specific diseases. Moreover, their ability to induce apoptosis and inhibit cell proliferation has made them promising candidates in cancer therapy, particularly for breast cancer [10]. Researchers have recently synthesized numerous chalcone analogues, demonstrating improved pharmacokinetics and reduced toxicity, suggesting that continued modification of these scaffolds could yield even more effective therapeutic agents [11].

This research aims to synthesize and evaluate new chalcone derivatives with enhanced biological activities against breast cancer cells (MCF-7) and pathogenic bacteria. The study investigates explicitly structural variations introduced through different substitutions on the chalcone scaffold and assesses their impact on cytotoxic and antibacterial properties. Additionally, molecular docking techniques are employed to predict interactions with key biological targets, providing a rationale for observed in vitro effects. The overarching objective is to establish a foundation for designing optimized chalcone-based therapeutic agents that are effective in cancer treatment and microbial resistance

2. Materials and Methods

2.1 Materials

In this study, all chemicals used were of high purity. Sigma-Aldrich and Merck companies obtained HCl (37%), 1-(4-hydroxyphenyl)ethan-1-one, and 2,4-dihydroxybenzaldehyde. Finally, 4-hydroxybenzaldehyde and NaOH were obtained from the BDH company.

2.2 Methods

Experimental Methods

Initially, an aqueous solution of sodium hydroxide (5% NaOH, 5.0 mmol) was added gradually to a round-bottomed flask containing 1,4-dicarbaldehyde-benzene (1.0 mmol) along with various substituted compounds, such as 1-(4-hydroxyphenyl)ethan-1-one, 2,4-dihydroxybenzaldehyde, 4-aminobenzaldehyde, and 4-hydroxybenzaldehyde (2.0 mmol). The solution was stirred for 24 hours. Since the reaction proceeded under mild conditions, prolonged stirring ensured complete condensation. Once the reaction reached completion, the mixture was carefully poured into ice-cold water. Subsequently, 5% hydrochloric acid was added dropwise until a noticeable precipitation of yellow solids occurred. The formation of these solids indicated successful product formation. Consequently, the resulting mixture was subjected to vacuum filtration, and the obtained solid residue was dried thoroughly to yield intermediates 1a-1d [12].

Chalcone Derivatives (1A and 1B) Antibacterial Activity Study

The cup-plate agar diffusion technique was used to evaluate the prepared chalcone derivatives for antibacterial activity, and the inhibition zone was measured in mL. The derivatives were compared to amoxicillin at 100 and 50 mg/ml for antibacterial activity. Antibacterial activity against *Bacillus subtilis* and *E. coli* was tested for these derivatives. The experiment used Muller-Hinton agar. Petri dishes were used to solidify sterilized agar. A sterilized triangular loop uniformly dispersed microbial suspensions on the press surface. Aseptic stainless-steel cylinders with 12 mm diameters created cavities. Micropipettes were used to inject synthetic chemicals at 100 and 50 M into the cavities. They were then allowed to disperse for an hour. All compounds were dissolved in DMSO, except pure ceftriaxone was in sterile distilled water. The plates were in a 37°C incubator for 48 hours. After incubation, the cups' inhibitory zone was measured in mL [13].

3. Results and Discussion

The synthesis mechanism of chalcone derivatives involved a base-catalyzed Claisen-Schmidt condensation between 1,4-benzenedicarbaldehyde (1.0 mmol) and various substituted compounds, specifically 1-(4-hydroxyphenyl)ethan-1-one, 2,4-dihydroxybenzaldehyde, 4-aminobenzaldehyde, and 4-hydroxybenzaldehyde (2.0 mmol). In this reaction, the carbonyl carbon of the aldehyde underwent nucleophilic attack by the enolate ion generated from the active methylene group of the ketone in basic medium, typically using NaOH or KOH in ethanol. Initially, a β-hydroxy ketone intermediate formed, which subsequently underwent dehydration to yield the corresponding α,β-unsaturated chalcone derivative. The resulting chalcones appeared as yellow to orange crystalline solids with high yields ranging from 70% to 90%, depending on the electronic nature of the substituents. Spectroscopic analysis using FTIR and NMR spectrometry confirmed the formation of the chalcone framework with characteristic peaks for the olefinic protons and carbonyl group. This synthetic approach proves efficient and versatile, as it accommodates various electron-donating or withdrawing groups on the aromatic rings, modulating the final products' conjugation and reactivity. Studies have shown that such structural diversity enhances chalcones' biological and photophysical properties. Therefore, this method remains a fundamental and broadly applicable route for synthesizing multifunctional chalcone derivatives.

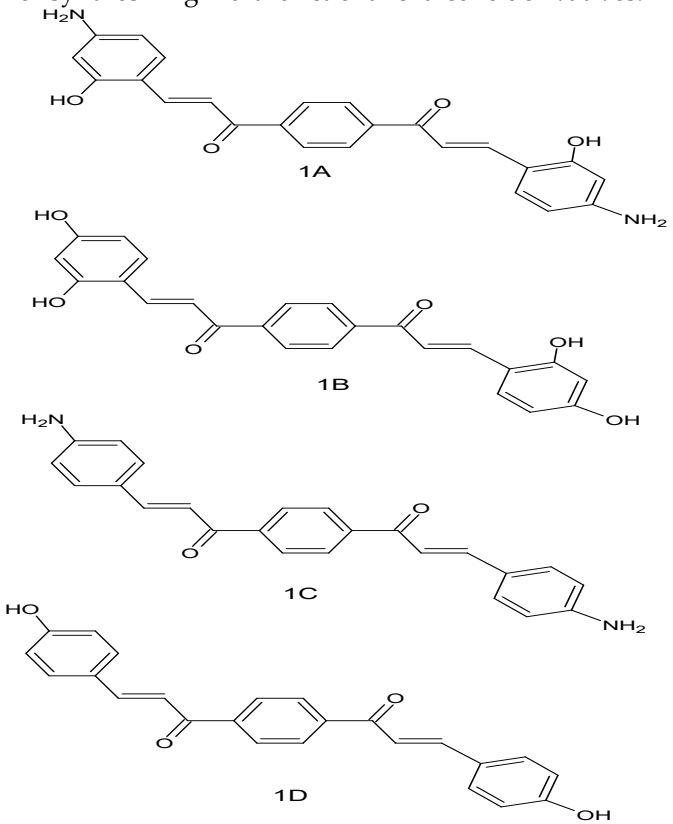

Figure 1. Chemical structures of chalcone derivatives 1A-1D.

The Physical chemistry properties of synthesized chalcone derivatives are listed in Table 1, exhibiting distinct physicochemical properties, as reflected by their molecular weights, melting points, and elemental compositions. The compound 1A, with the molecular formula $C_{24}H_{20}N_2O_4$, has a molecular weight of 400.43 g/mol and displays a melting point in the range of 263–267 °C. The high nitrogen (7.00%) and oxygen (15.98%) content suggests the presence of multiple polar functional groups such as amines and carbonyls, which can enhance hydrogen bonding and potentially improve solubility and biological activity.

Compound 1B, with a formula of $C_{24}H_{18}O_6$ and a molecular weight of 402.40 g/mol, exhibits the highest oxygen percentage (23.86%), indicative of an increased number of hydroxyl or carbonyl groups, which might enhance antioxidant or radical-scavenging activity. Its relatively lower melting point (231–235 °C) compared to 1A suggests weaker intermolecular interactions, possibly due to the absence of nitrogen atoms.

Compound 1C ($C_{24}H_{18}N_2O_2$), the lightest among the three (368.44 g/mol), shows the highest carbon content (78.24%) and lower oxygen content (8.68%), indicating a more hydrophobic nature. The melting point of 209–213 °C reflects reduced lattice stability, possibly due to the simpler structure or less hydrogen bonding capability. Notably, nitrogen (7.60%) and a relatively low oxygen content suggest structural modifications that may enhance lipophilicity and membrane permeability, which could explain its higher cytotoxicity in MCF-7 cells compared to 1A.

Compound 1D, with a formula of $C_{24}H_{16}O_4$ and a molecular weight of 402.40 g/mol, exhibits the highest oxygen percentage (17.28%), indicative of an increased number of hydroxyl or carbonyl groups, which might enhance antioxidant or radical-scavenging activity. Its relatively lower melting point (240–244 °C).

Table 1. Physical chemistry properties of synthesized derivatives.

No.	Chemical formula	Molecular weight	M.P. (°C)
1A	$C_{24}H_{20}N_2O_4$	400.434	263-267
1B	$C_{24}H_{18}O_6$	402.402	231-235
1C	$C_{24}H_{18}N_2O_2$	368.436	209-213
1D	$C_{24}H_{16}O_4$	368.37	240–244

Discussion of FTIR Spectra of Chalcone Derivatives 1A-1D

The FTIR analysis of the synthesized chalcone derivatives confirmed the presence of key functional groups associated with the chalcone structure. A strong absorption band was observed for the carbonyl stretching of the α,β-unsaturated ketone, alongside broad bands indicating hydroxyl group stretching from phenolic substituents. Additional peaks corresponding to aromatic C=C stretching vibrations were also detected, supporting an extended conjugated system. In the proton NMR spectra, the olefinic protons exhibited typical coupling patterns consistent with a trans-configuration, while aromatic protons appeared as overlapping signals in the downfield region. Broad singlets corresponding to the hydroxyl protons were also observed. In the ^{13}C-NMR spectra, signals were recorded for the carbonyl carbon of the enone system, along with distinct peaks for aromatic and olefinic carbons. These spectroscopic results collectively confirm the successful formation of the chalcone core, incorporating both the aromatic moieties and the conjugated enone functionality.

The FTIR spectrum of compound 1A shows a broad absorption band at 3325 cm^{-1}, which is attributed to the stretching vibrations of hydroxyl (–OH) group. The peak observed at 2989 cm^{-1} corresponds to aliphatic C–H stretching [14]. A strong and sharp absorption at 1714 cm^{-1} confirms the presence of the α,β-unsaturated carbonyl group (C=O) of the chalcone framework. The band at 1626 cm^{-1} indicates α,β-C=C stretching. Additional peaks at 1401 and 1250 cm^{-1} are associated with C–N and C–O stretching, while the bands below 1000 cm^{-1} correspond to out-of-plane aromatic C–H bending vibrations.

This spectral profile supports the successful synthesis of 1A containing phenolic, amine, and enone functional groups [15], as shown in Figure 2.

The FTIR spectrum of compound 1B exhibits a broad band around 3354 cm^{-1}, indicating the presence of a hydroxyl group, likely due to phenolic functionalities. Peaks at 2932 and 2865 cm^{-1} correspond to aliphatic C–H stretching vibrations. The sharp absorption at 1722 cm^{-1} is characteristic of the carbonyl (C=O) group, while the band at 1621 cm^{-1} is attributed to α,β-C=C stretching [16]. The presence of bands at 1439, 1250, and 1181 cm^{-1} supports the existence of C–O stretching, particularly from phenolic and enolic components. Peaks below 1000 cm^{-1} (especially around 830 and 579 cm^{-1}) indicate out-of-plane C–H bending. These results confirm that compound 1B retains the characteristic features of chalcone derivatives substituted with hydroxyl groups [17], as shown in Figure 3.

In the FTIR spectrum of compound 1C, a strong and broad band appears at 3287–3225 cm^{-1}, overlapping N–H stretching vibrations. Peaks at 2980 and 2905 cm^{-1} correspond to C–H stretching of aliphatic chains. The sharp peak at 1718 cm^{-1} corresponds to the chalcone moiety's carbonyl (C=O) stretching. The α,β- of C=C stretching is observed at 1618. The presence of bands at 1405 and 1235 cm^{-1} indicates C–N and C–O stretching vibrations [18]. A strong absorption around 1023 cm^{-1} and peaks below 800 cm^{-1} represent aromatic out-of-plane bending [19], as shown in Figure 4.

In the FTIR spectrum of compound 1D, a strong and broad band appears at 3429 cm^{-1}, overlapping O–H stretching vibrations. Peaks at 2954 and 2854 cm^{-1} correspond to C–H stretching of aliphatic chains. The sharp peak at 1715 cm^{-1} corresponds to the chalcone moiety's carbonyl (C=O) stretching. The α,β- of C=C stretching is observed at 1622. The presence of bands at 1209 cm^{-1} indicates C–O stretching vibration [18]. A strong absorption around 1052 cm^{-1} and peaks below 800 cm^{-1} represent aromatic out-of-plane bending [19], as shown in Figure 5.

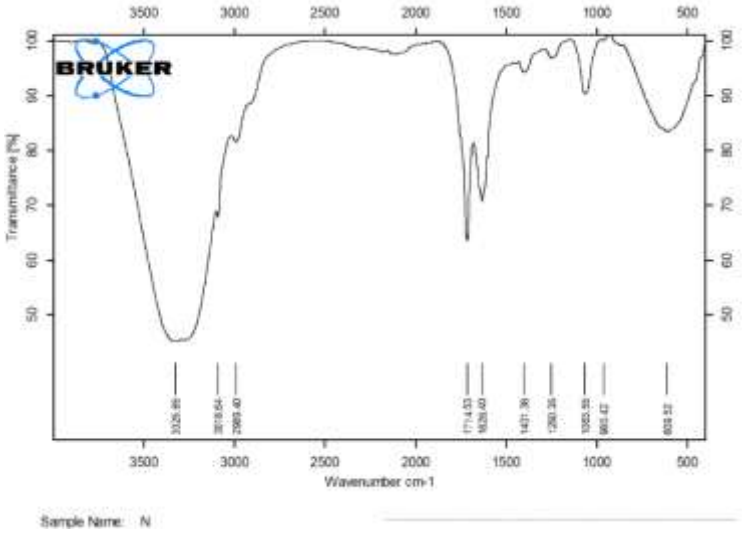

Figure 2. FTIR spectrum of derivative 1A

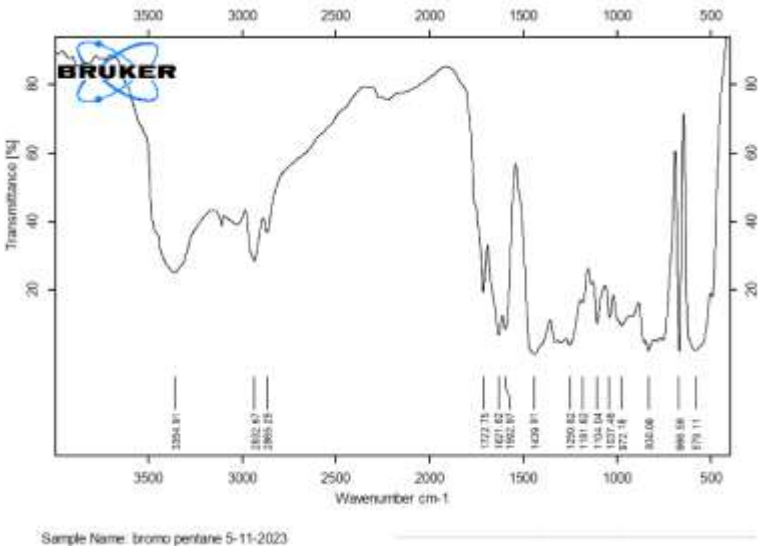

Figure 3. FTIR spectrum of derivative 1B.

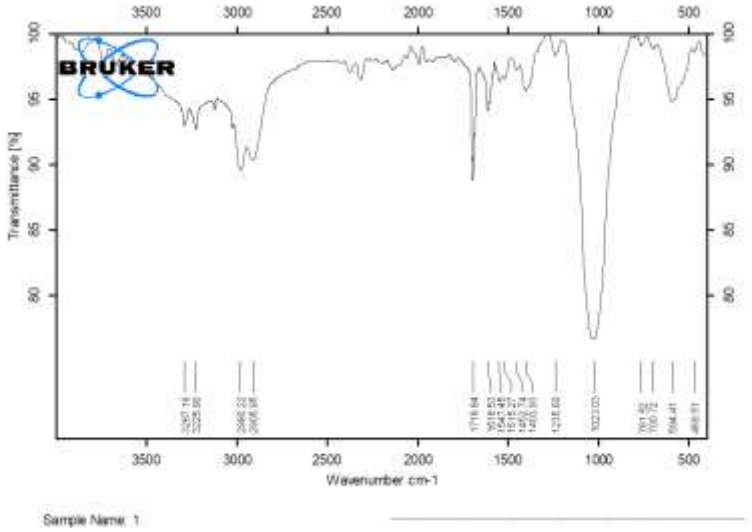

Figure 4. FTIR spectrum of derivative 1C.

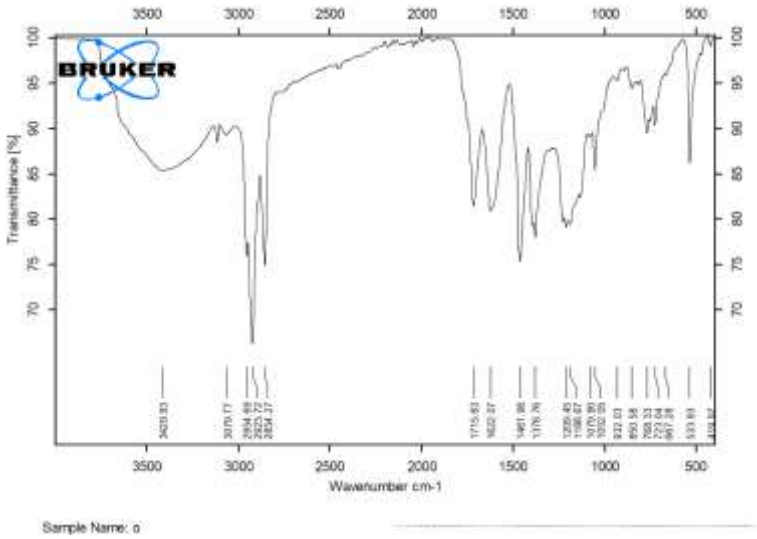

Figure 5. FTIR spectrum of derivative 1D.

Discussion of ^{1}H NMR Spectra of Chalcone Derivatives 1A-1C

For derivative 1A, the ^{1}H NMR spectrum revealed multiple aromatic signals between δ 7.04-8.23 ppm, corresponding to protons on the substituted aromatic rings. A downfield singlet around δ 9.11 ppm was observed, which can be attributed to a hydroxyl proton in

hydrogen bonding. The multiplet pattern in the aromatic region confirms the presence of multiple proton environments. A signal at δ ~4.97 ppm likely belongs to protons (NH_2 or OH), while the protons of α,β-unsaturated at δ 6.95 and 6.97 [20], as shown in Figure 6.
In the case of derivative 1B, the spectrum showed aromatic proton signals between δ 7.00-8.26 ppm, with some overlap due to the symmetric nature of the rings. A downfield peak around δ 9.2 ppm is consistent with the hydroxyl proton of a catechol moiety [21], suggesting strong hydrogen bonding, while the protons of α,β-unsaturated at δ 6.98 and 6.99, as shown in Figure 7.

The ^{1}H NMR spectrum for derivative 1C exhibited a similar aromatic region δ 7.30-8.10 ppm, with characteristic multiplets corresponding to the phenyl and amino-substituted phenyl rings. Unlike 1A and 1B, no strong downfield hydroxyl signals were present, consistent with the absence of OH groups in this derivative [22]. A moderate singlet at δ ~4.48 ppm likely represents an exchangeable NH_2 proton, while the protons of α,β-unsaturated at δ 6.68-6.70, as shown in Figure 8.

The ^{1}H-NMR spectrum shows a broad singlet at 9.38 ppm, attributed to phenolic OH protons. Aromatic protons resonate between 6.8-8.2 ppm, confirming a multi-ring aromatic system. The splitting patterns suggest substitution on the aromatic rings. No aliphatic proton signals are present, supporting the fully aromatic nature. The spectrum aligns with the proposed structure, which includes hydroxyl, carbonyl, and conjugated aromatic systems, as shown in Figure 9.

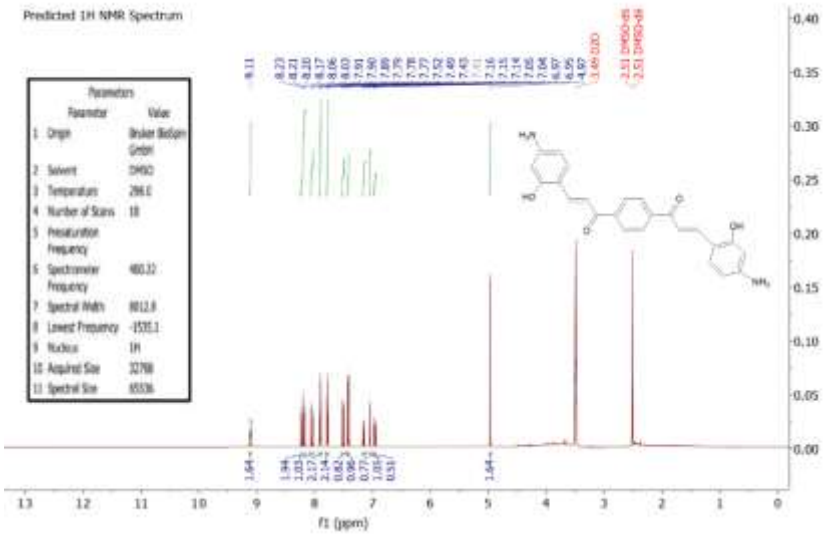

Figure 6. ^{1}H-NMR spectrum of derivative 1A.

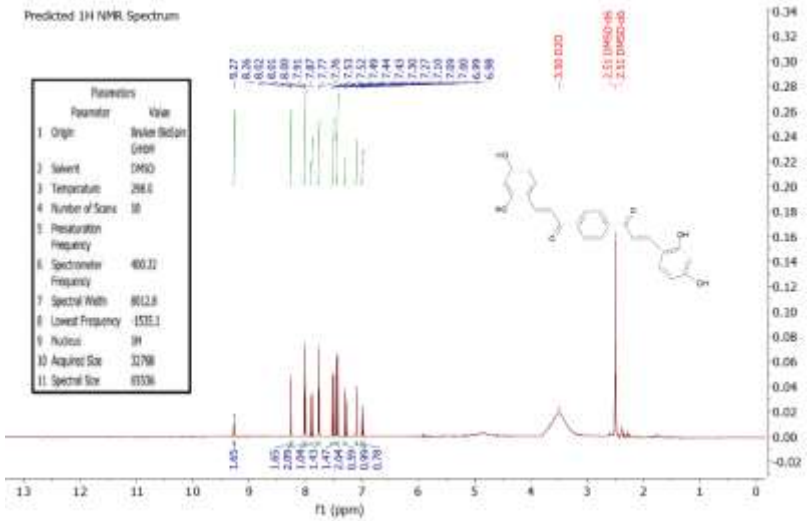

Figure 7. [1]H-NMR spectrum of derivative 1B.

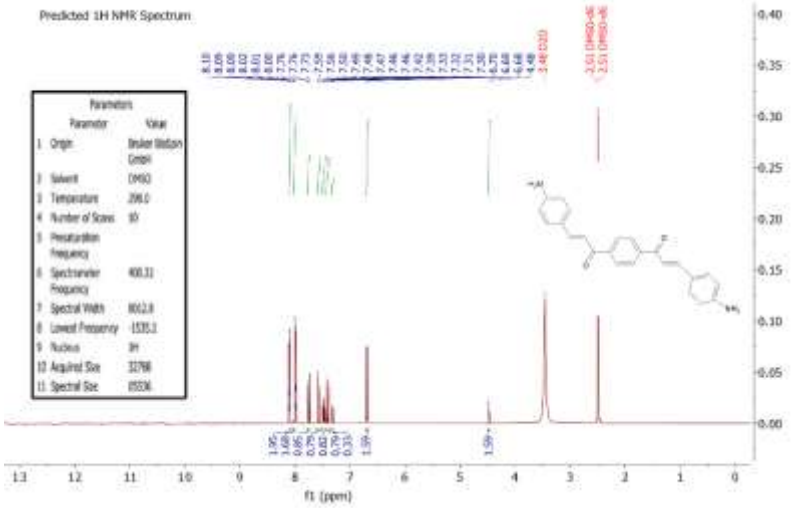

Figure 8. [1]H-NMR spectrum of derivative 1C.

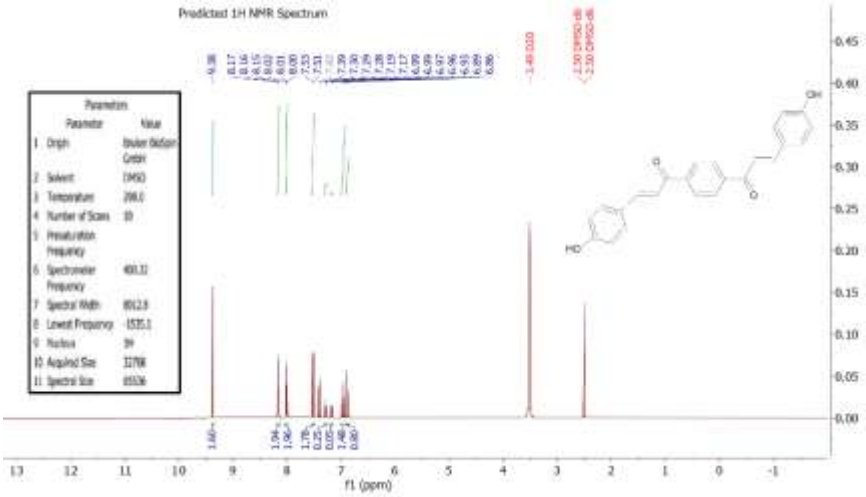

Figure 9. [1]H-NMR spectrum of derivative 1D.

Discussion of [13]C-NMR Spectra of Chalcone Derivatives 1A-1C

For chalcone derivative **1A**, the [13]C NMR spectrum exhibited characteristic signals clearly identifiable for aromatic and carbonyl carbons. Peaks appearing downfield around δ 187-188 ppm are assigned to the conjugated carbonyl carbons, typical for α,β-unsaturated ketones. Aromatic carbon resonances were observed predominantly between δ 101 and δ 160 ppm, reflecting various aromatic substitution patterns [23]. These shifts are consistent with aromatic carbons adjacent to electronegative substituents like amino and hydroxyl groups, corroborating the proposed structural configuration, as shown in Figure 10.

In derivative **1B**, two distinctive carbonyl signals emerged near δ 188 ppm, again indicative of the α,β-unsaturated carbonyl functionality. Aromatic carbon resonances appeared broadly between δ 102 and δ 161 ppm, aligning with hydroxyl substitutions enhancing electron density distribution across the aromatic systems [24]. These findings were consistent with typical chemical shifts reported in the literature for chalcone derivatives containing multiple hydroxyl functionalities, as shown in Figure 11.

For compound **1C**, the carbonyl carbon was clearly detected at δ 190 ppm, slightly more downfield than in 1A and 1B, reflecting subtle electronic variations due to the absence of hydroxyl substituents. Aromatic carbon signals clustered between δ 116 and δ 150 ppm, confirming the expected aromatic environment influenced by amino groups. The spectrum distinctly supports the presence of electron-donating groups, controlling the

electron density distribution across the aromatic rings as previously described in similar chalcone analogs [25], as shown in Figure 12.

For compound **1D**, the ^{13}C-NMR spectrum at displays distinct signals indicating the presence of carbonyl groups around 190 ppm, confirming ketone or ester functionalities. Aromatic carbon signals appear between 110–160 ppm, suggesting multiple non-equivalent benzene rings. The pattern and number of signals are consistent with the compound's asymmetric structure, and no aliphatic carbons are observed except for residual solvent peaks from DMSO, as shown in Figure 13.

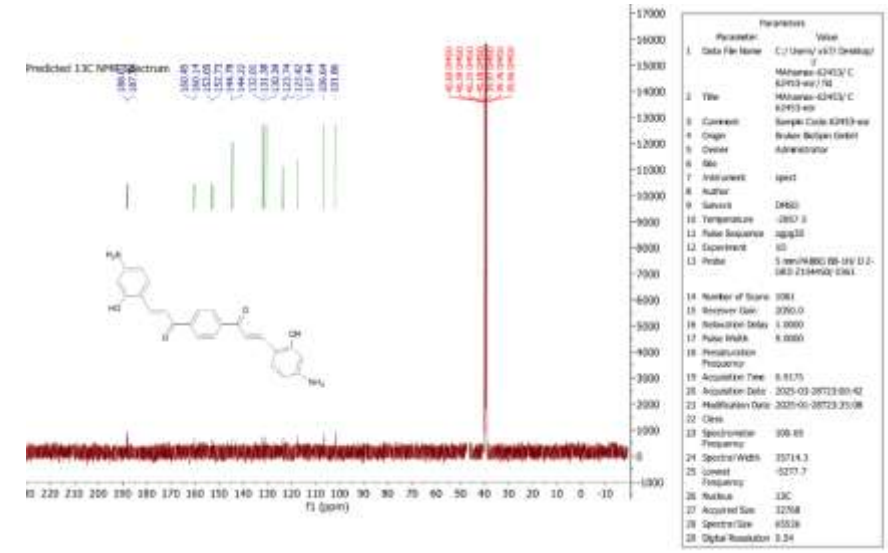

Figure 10. ^{13}C-NMR spectrum of derivative 1A.

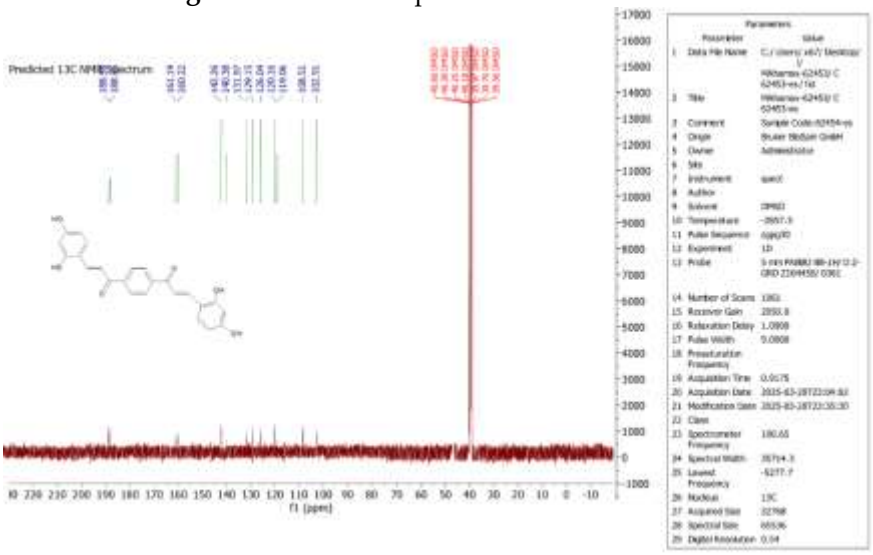

Figure 11. ^{13}C-NMR spectrum of derivative 1B.

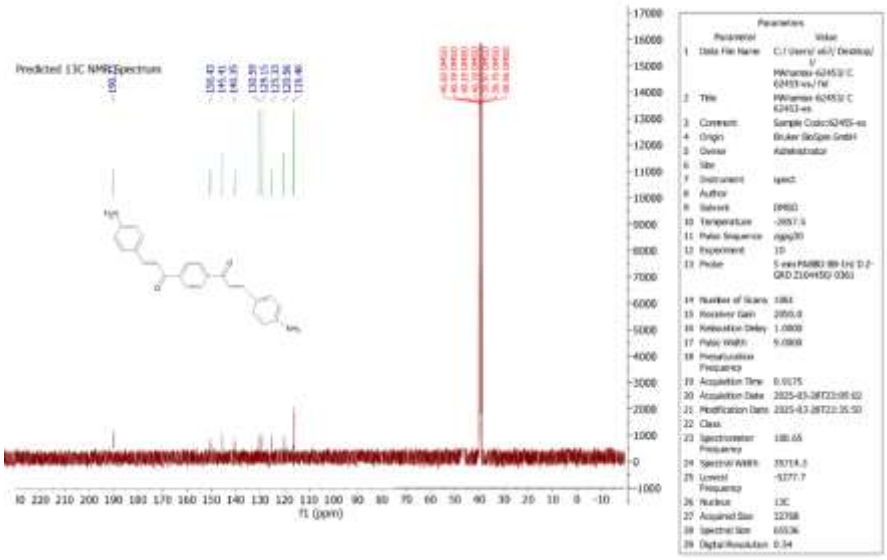

Figure 12. ^{13}C-NMR spectrum of derivative 1C.

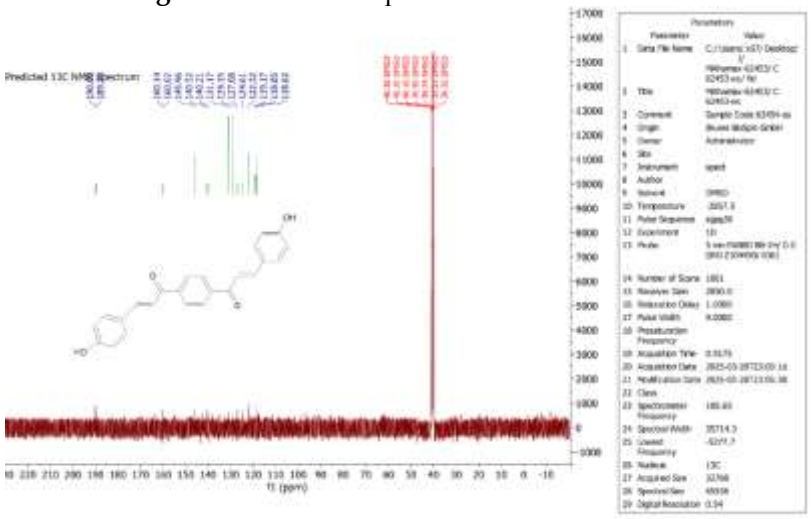

Figure 13. ^{13}C-NMR spectrum of derivative 1D.

The antibacterial activities of synthesized chalcone derivatives are evaluated against three bacterial strains: *Bacillus subtilis*, *Escherichia coli*, and *Streptococcus pneumoniae*, as shown in Figures 14-16. The inhibition zones clearly indicate a dose-dependent response, where the compounds exhibit greater activity at 100 μg/mL compared to 50 μg/mL. In the case of *B. subtilis*, compound 1A achieves the highest inhibition zone of 25 mm, surpassing both the standard sulfadiazine (20 mm) and compound 1B (22 mm), thus demonstrating superior potency. Against *E. coli*, 1A again shows remarkable efficacy with a 27 mm zone of inhibition, significantly higher than sulfadiazine (23 mm) and 1B (23 mm), suggesting broad-spectrum activity. Similarly, against *S. pneumoniae*, compound A1 records the highest activity (18 mm), outperforming the standard and compound 1B. These findings indicate that structural modifications in chalcone derivatives can enhance their antimicrobial properties. Moreover, all synthesized compounds demonstrate improved antibacterial effects compared to the reference drug at both concentrations, emphasizing their potential as alternative therapeutic agents. The consistently stronger performance at 100 μg/mL supports the idea that increased concentration leads to greater membrane disruption or intracellular targeting by the compounds. Overall, the data confirm that these chalcone derivatives possess promising antibacterial potential.

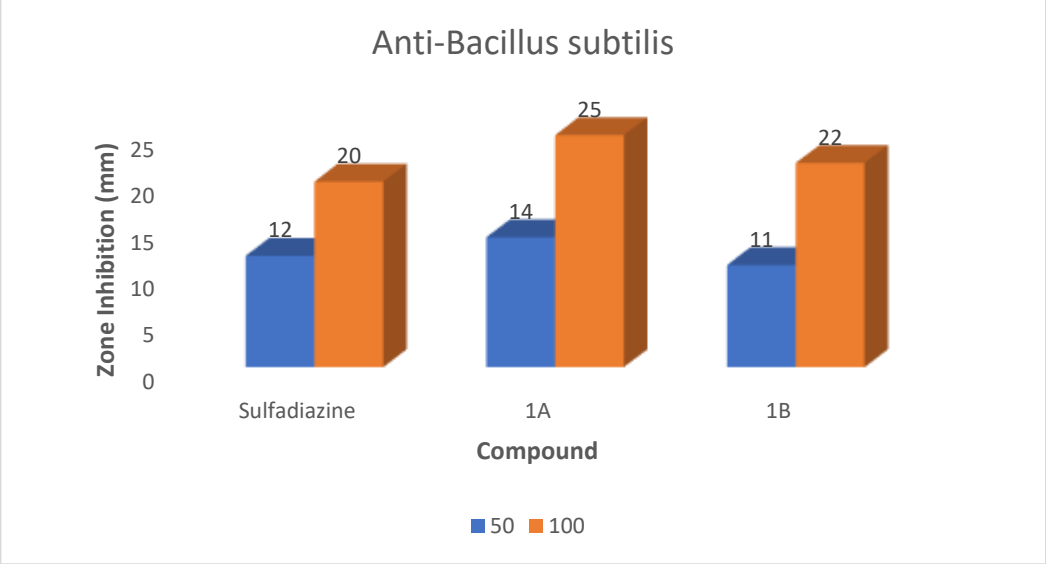

Figure 14. Biological activity of derivatives against *Bacillus subtilis*.

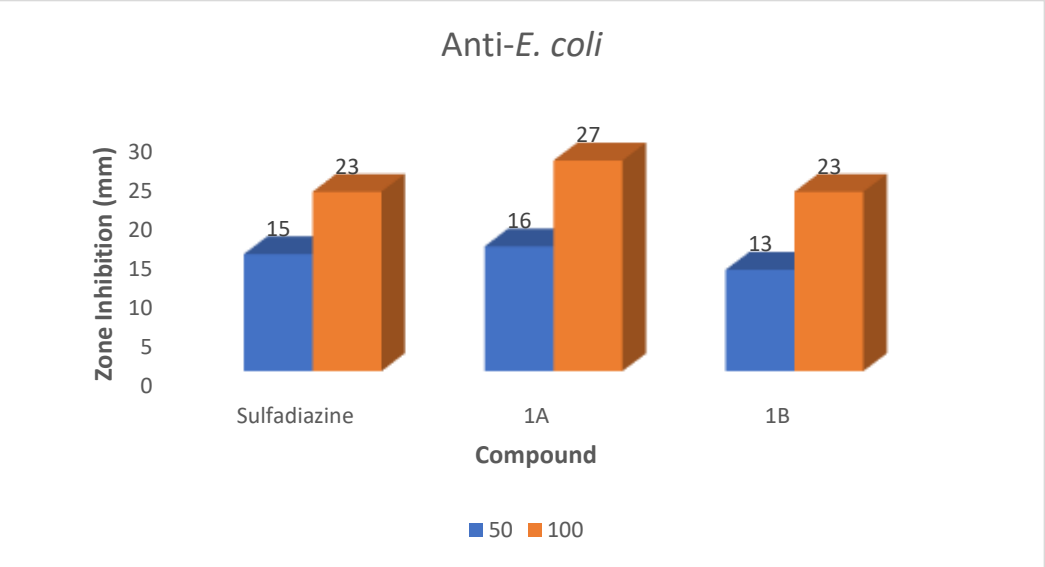

Figure 15. Biological activity of derivatives against *E. Coli*.

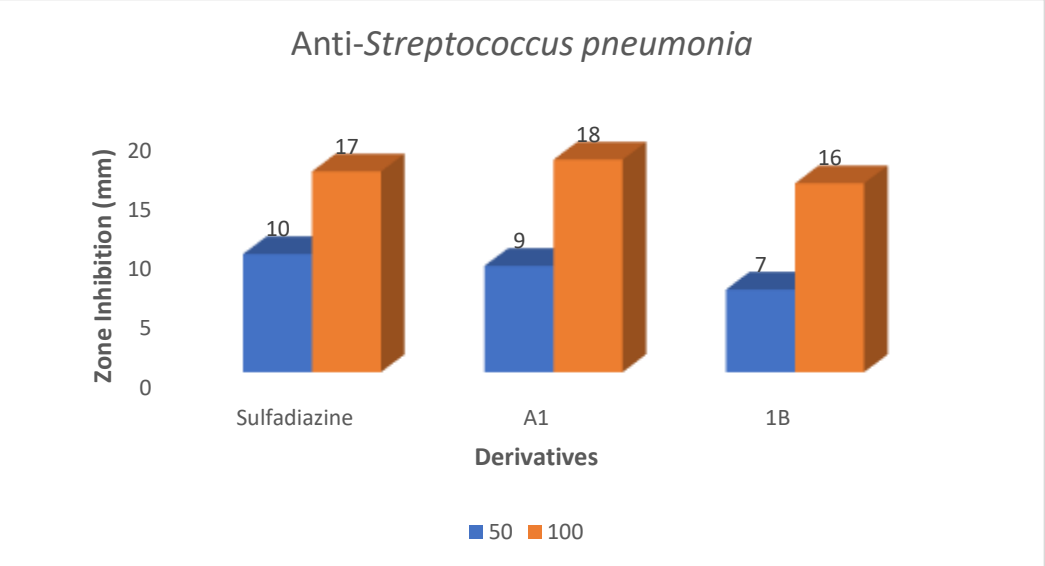

Figure 16. Biological activity of derivatives against *Streptococcus pneumoniae*.

The cytotoxic activity of the synthesized chalcone derivatives 1A and 1C was evaluated against the MCF-7 breast cancer cell line using the MTT assay across a range of

concentrations (0–320 PPM). The results showed a concentration-dependent decrease in cell viability for both derivatives. At lower concentrations, 1A and 1C maintained over 85% viability; however, a significant reduction was observed with increasing concentration. Derivative 1C exhibited more potent cytotoxicity compared to 1A, particularly at higher concentrations. At 320 PPM, cell viability dropped to approximately 10.93% for 1C, while 1A showed a viability of 19.13%, indicating the greater potency of 1C, as listed in Table 2 and Figures 17-20.

These findings suggest that the presence and position of substituents on the aromatic ring may influence the anticancer activity of chalcones. This aligns with previous studies that reported enhanced cytotoxic effects for chalcone derivatives possessing electron-withdrawing groups. The observed cytotoxicity may be attributed to the ability of these compounds to induce apoptosis and disrupt mitochondrial function in cancer cells.

Previous studies have consistently demonstrated the potent anticancer activity of chalcone derivatives against MCF-7 breast cancer cells. For instance, Priya, S., and *et al.*, (2025) reported that chalcones bearing electron-withdrawing substituents, such as nitro or halogen groups, showed enhanced cytotoxicity due to improved cellular uptake and apoptosis induction [26]. Similarly, Santos, T. et al. (2024) observed that methoxy-substituted chalcones effectively inhibited MCF-7 cell proliferation [27]. In another investigation, Mirzaei, H., & Emami, S. (2016) synthesized fluorinated chalcone analogs that exhibited IC_{50} values below 25 μM against MCF-7, attributing their activity to tubulin polymerization inhibition [28]. Furthermore, Zhu, M., and *et al*., (2018), confirmed that the α,β-unsaturated ketone moiety present in chalcones plays a key role in binding to cellular thiols and disrupting mitochondrial pathways [29]. These findings collectively support the rationale for designing new chalcone derivatives with varied substitution patterns to enhance their anticancer potential against MCF-7 cells.

Table 2. IC50 rates of derivatives 1A and 1C NPs on MCF-7 cell viability.

Concentration (PPM)	**1A**		**1C**	
	Mean	SD	Mean	SD
0	100.9808	4.563203	100.831	2.485501
20	90.673	3.295475	87.74167	2.486013
40	71.46767	2.264617	72.27687	1.272439
80	60.44367	2.176861	55.29967	2.309485
160	36.258	0.920821	22.037	2.777286
320	19.12833	2.540484	10.93433	1.532822

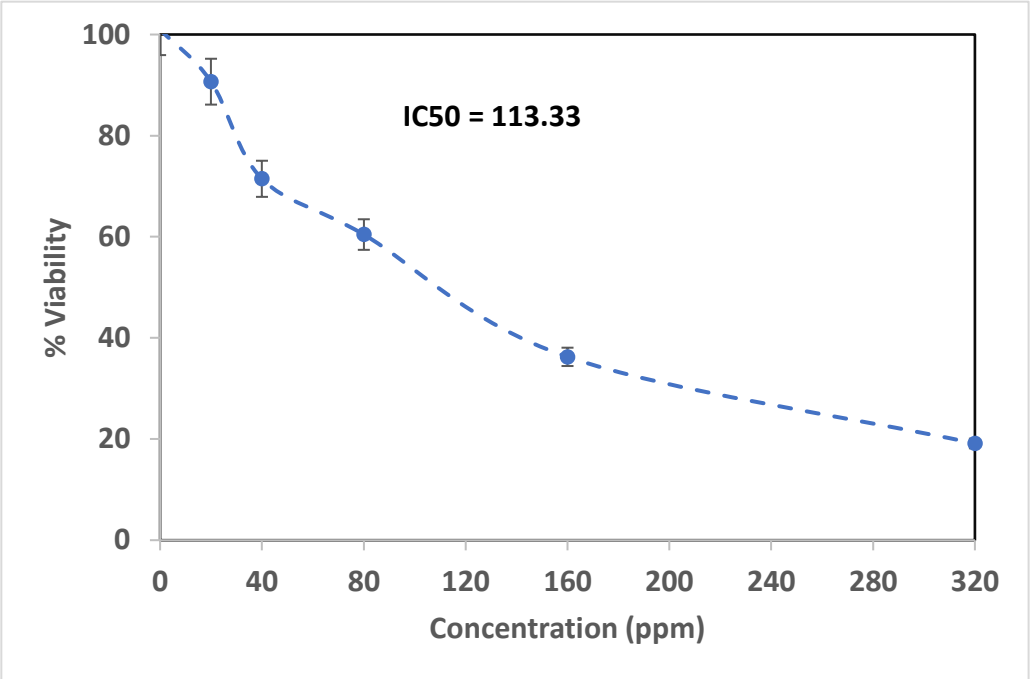

Figure 17. IC50 of derivative 1A.

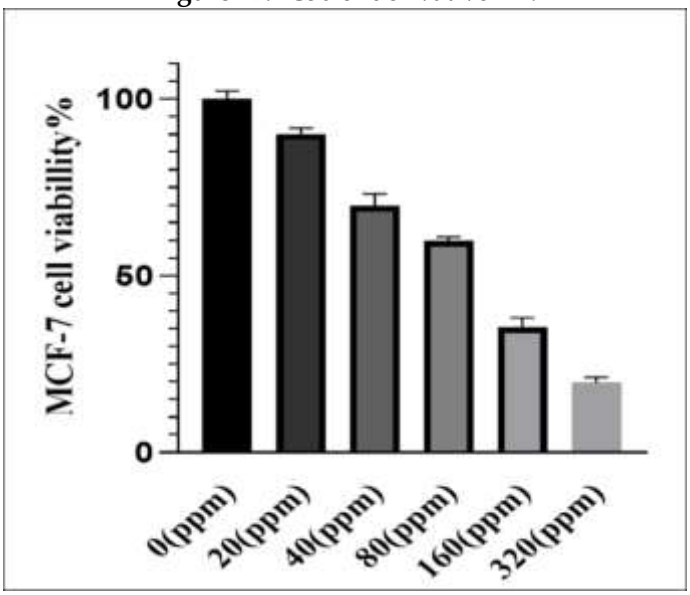

Figure 18. Effect of derivative 1A against MCF-7.

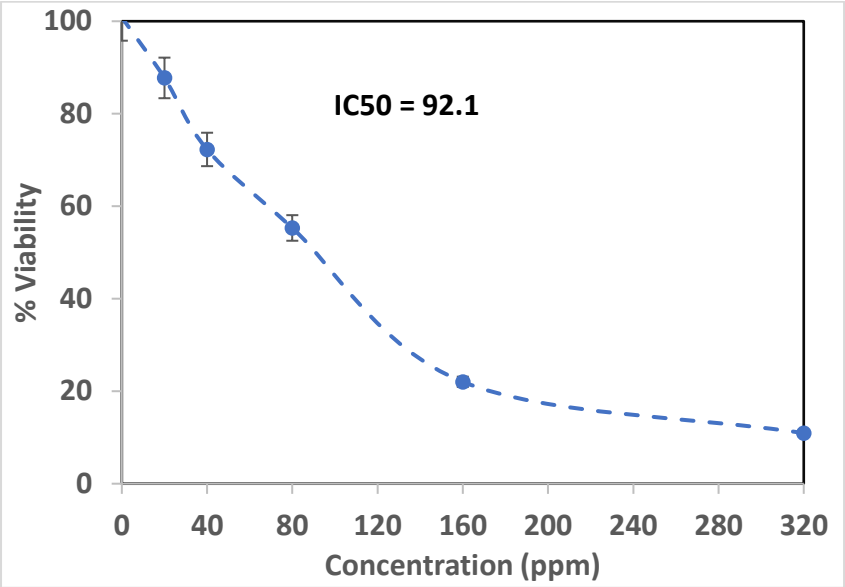

Figure 19. IC50 of derivative 1C.

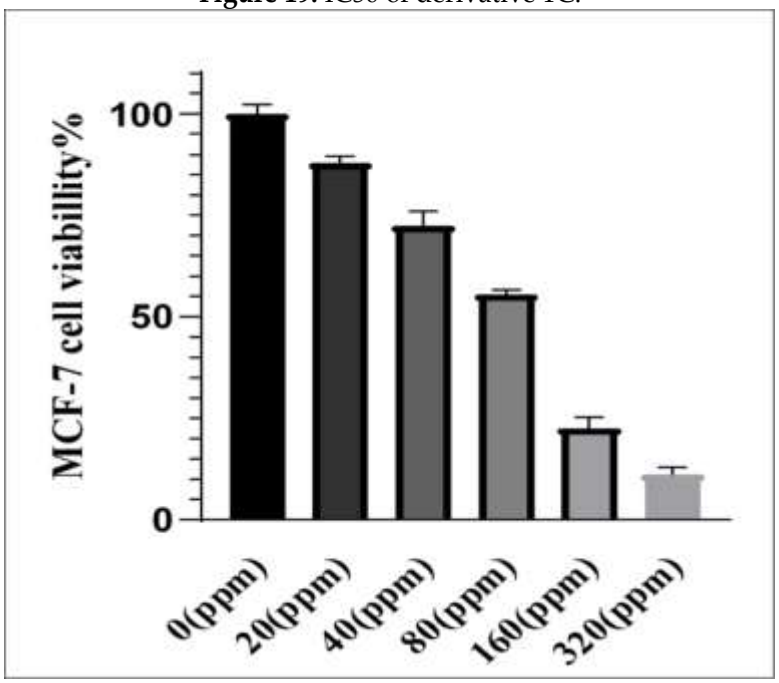

Figure 20. Effect of derivative 1C against MCF-7.

Molecules Library Preparation

After synthesizing and characterizing the novel derivative (1C), Chemdraw Ultra 12.0 (https://chemdraw pro.software.informer.com/12.0/) was used to build the 3D structures and minimize energy. Using Hyperchem 8.08, semi-empirical AM1 pre-optimized the structures. Using the B3LYP/6-31G basis set, density functional theory DFT optimized the structures for the most stable conformation. By default, maximum force, root-mean-square (RMS) force, maximum displacement, and RMS displacement converge to "YES". All ligand vibrational frequency measurements are positive, indicating stability. The optimized structures were merged in one database using MOE software (2022) to analyze ligand affinity (Figure 21). Figure 22 schematically shows the docking, ligand analysis, and reactivity process [30].

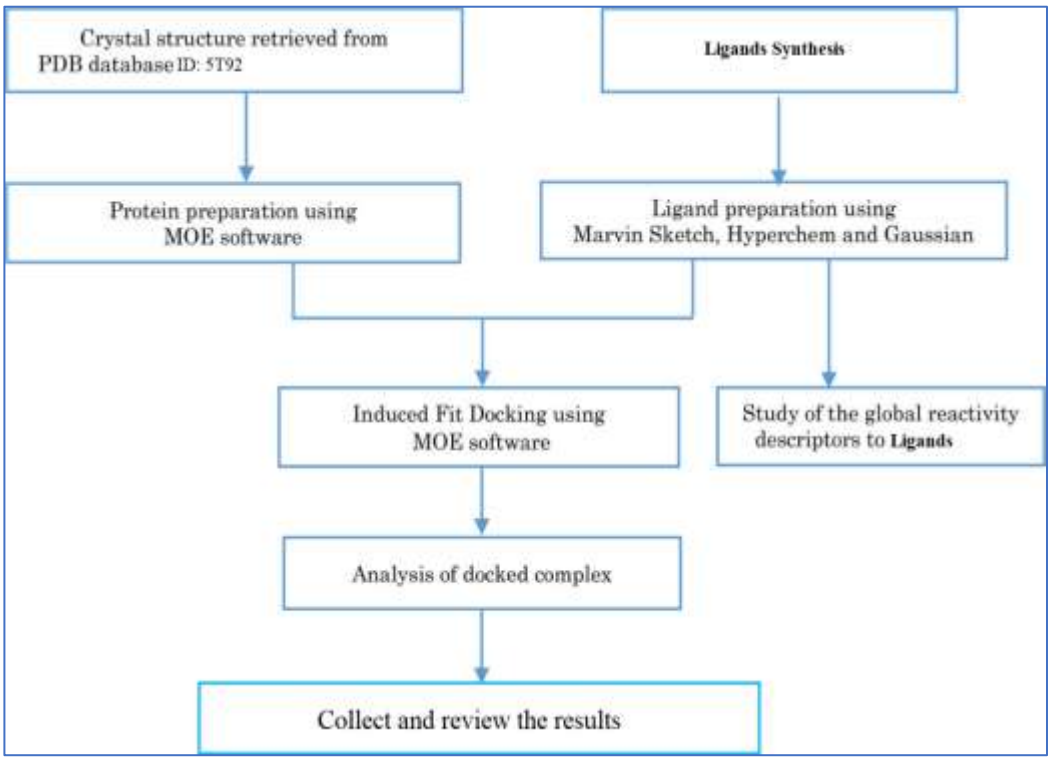

Figure 21. Schematic representation of the docking procedure, analysis of ligands and reactivity.

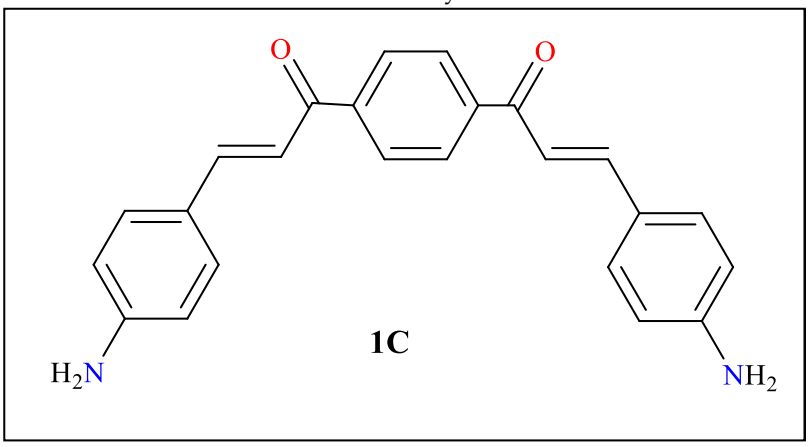

Figure 22. 2D structures of the selected compound (ligand).

Preparation of Receptor

The structure of the (ESTROGEN RECEPTOR ALPHA ligand binding domain in complex with (2E)-3-{4-[(1R)]-2-(4-fluorophenyl)-6-hydroxy-1-methy l-1,2,3,4-tetrahydroisoquinolin-1-yl]phenyl}prop-2-enoic acidprop-2-enoic acid) (PDB ID: 5T92) (Figure 23) was selected from the Protein Data Bank. Given the importance of the water molecule at the active site of the enzyme for forming a hydrogen bond, it was added for that purpose. Subsequently, the protein structure was generated by repairing the bonds that were lost due to X-ray diffraction and adding hydrogen atoms. It is worth noting that PDB is known worldwide for the accuracy of biological macromolecule crystal structures [31].

Note: The 5T92 protein, which contains the ligand-binding domain of the Estrogen Receptor alpha (ERα), is critical for developing and progressing ER$^+$ breast cancer [32]. When ERα binds to estrogen, it activates cell growth and survival genes. In hormone-dependent breast cancer, ERα overexpression or activation leads to uncontrolled cell proliferation, making it a crucial therapeutic target. A well-characterized binding location and importance to hormone-driven breast cancer led to its selection for molecular docking, enabling in silico screening of putative ERα antagonists.

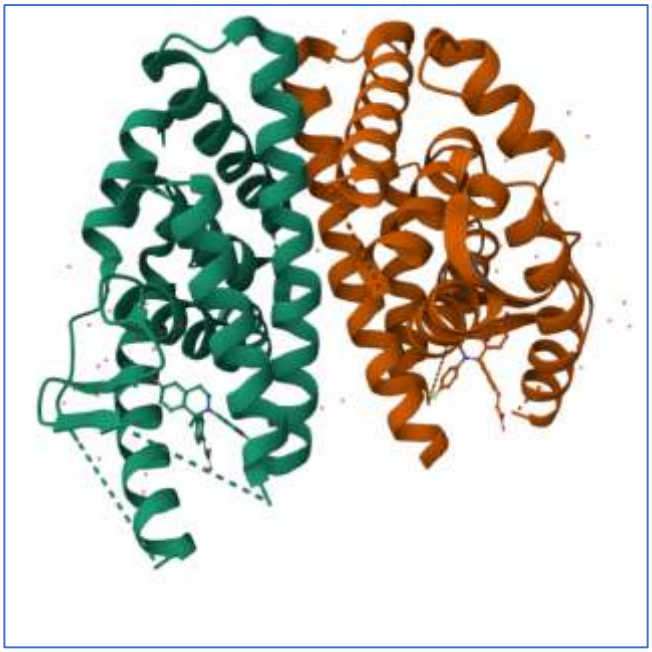

Figure 23. Crystal structures of the 5T92 protein.

Ligand-Protein molecular docking

MOE was used for all docking and scoring computations (2022). Estrogen receptor alpha ligand binding domain crystal structure in combination with (2E)-3-{4-[(1R)-2-(4-fluorophenyl)-6-hydroxy-1-methy-l-1,2,3,4-tetrahydroisoquinolin-1-yl]phenyl} (PDB ID: 5T92) (Figure 23) was retrieved from the Protein Data Bank at 2.22 Å resolution. A resolution of 1.5 to 2.5 Å is favorable for docking investigations. The optimal RMSD score is about 2 Å with an energy score below -7 kcal/mol. These two values are typically used to confirm molecular docking results.

Molecular Docking Results

Molecular docking is a technique that is usually employed in the early stages of drug discovery. In this case, all molecular docking computations were carried out using MOE software, and the binding modes of the derivative (1C) to the protein (5T92) were subsequently predicted (Figure 24). Their predicted binding affinities and features are listed for the investigated derivative (1C) and (5T92) in Table 3, while Table 4 presents the best binding poses of derivative (1C) against the target protein.

The following figures and tables illustrate the 2D and 3D representations of interactions of the inspected compounds with the key amino acid residues of the (5T92) protein. Compounds **(1C)** showed good binding affinity values (Table 4 and Table 5) with protein (PDB ID: 5T92). The binding and mode of interactions of the derivative **(1C)** with the (PDB ID: 5T92) protein are shown in 2D and 3D figures. It has been demonstrated from the interactions that there are primarily different types of interactions (hydrogen bonding and hydrophobic interactions). Further analysis for the active site included examining bond lengths and hydrogen bonds, illustrated in the following figures. From these figures, it was observed that derivative (1C) interacts with various residue amino acids in several distinct ways: as a hydrogen donor, as a hydrogen acceptor, and pi-H acceptor and two pi-H interactions with water and several amino acids, two of which were also in the form of H-acceptor interactions. The relevant metrics for distance and energy in binding interaction are tabulated in Table 5.

Table 3. The binding affinity and rmsd result of **the 5T92** protein from the docking process.

Compounds	Binding Affinity Kcal/mol	Rmsd (Å)	E_conf	E_place	E_score1	E_refine	E_score 2

1C-pose1	-7.69461	2.029808	-5.78414	-11.7547	-9.434	-32.5248	-7.69461
1C-pose2	-6.59879	3.021166	-12.9605	-13.945	-8.55091	-31.8586	-6.59879
1C-pose3	-6.49097	1.689928	-6.25798	-13.419	-8.58693	-29.9599	-6.49097
1C-pose4	-6.40902	2.43953	10.47421	-11.619	-9.42748	-21.9059	-6.40902
1C-pose5	-6.40334	2.96115	-7.27107	-13.1953	-9.17146	-31.8333	-6.40334
Standard	-7.91706	2.137427	-93.9605	-102.304	-11.9107	-36.5557	-7.91706

Table 4. Smiles of selected ligand.

Compounds	Binding Affinity Kcal/mol	Rmsd (Å)	Smile
1C-pose1	-7.69461	2.029808	O=C(/C=C/c1ccc(N)cc1)c1ccc(C(=O)/C=C/c2ccc(N)cc2)cc1
1C-pose2	-6.59879	3.021166	O=C(/C=C/c1ccc(N)cc1)c1ccc(C(=O)/C=C/c2ccc(N)cc2)cc1
1C-pose3	-6.49097	1.689928	O=C(/C=C/c1ccc(N)cc1)c1ccc(C(=O)/C=C/c2ccc(N)cc2)cc1
1C-pose4	-6.40902	2.43953	O=C(/C=C/c1ccc(N)cc1)c1ccc(C(=O)/C=C/c2ccc(N)cc2)cc1
1C-pose5	-6.40334	2.96115	O=C(/C=C/c1ccc(N)cc1)c1ccc(C(=O)/C=C/c2ccc(N)cc2)cc1
Standard	-7.91706	2.137427	O=C(/C=C/c1ccc(N)cc1)c1ccc(C(=O)/C=C/c2ccc(N)cc2)cc1

Table 5. Details of the best poses of ligands (1C) with protein 5T92.

Compounds	Binding Affinity Kcal/mol	Rmsd (Å)	Atom of compound	Atom of Receptor	Involved receptor residues	Type of interaction bond	Distance (Å)	E (kcal/mol)
1C-pose1	-7.69461	2.029808	6-ring 6-ring	CG2 CD1	THR 347 PHE 404	(A) pi-H (A) pi-H	4.37 4.05	-0.7 -0.8
Standard	-7.91706	2.137427	O1147	OE1	GLU 353	(A) H-donor	2.53	-3.8

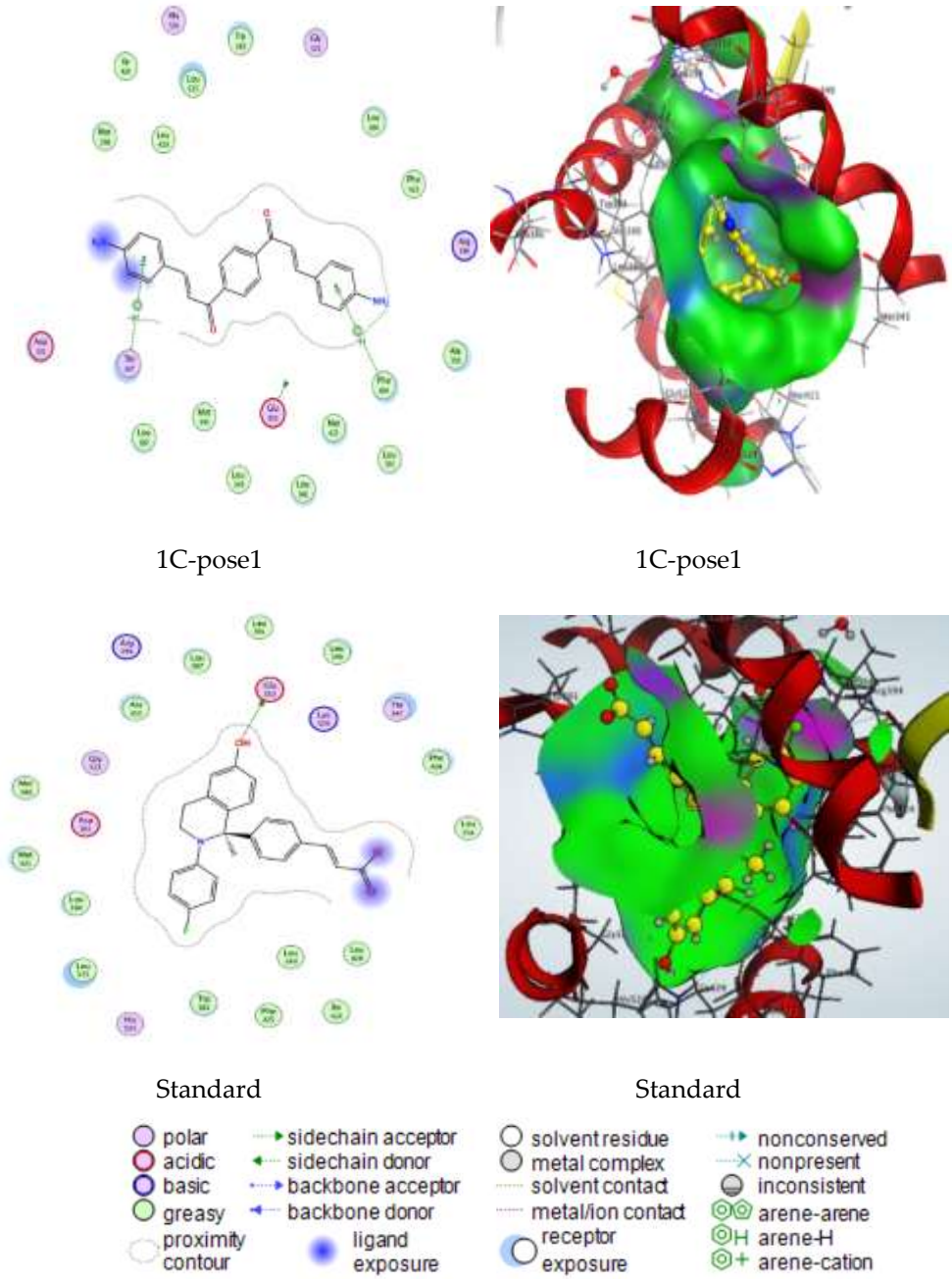

Figure 24. 2D and 3D of the best poses.

Interpretation of molecular docking results

The docking study of derivative 1C (pose1) compared to the standard ligand with respect to the 5T92 protein provides significant insights into their binding efficacy and interaction stability. Regarding binding affinity, 1C-pose1 attained a score of –7.69461 kcal/mol, while the reference molecule had a somewhat superior affinity of –7.91706 kcal/mol. This indicates that although derivative 1C binds well to the target region, the standard ligand has a more robust overall interaction with the protein according to free energy values.

Regarding RMSD, which quantifies the spatial alignment of the docked pose with the ideal orientation, 1C-pose1 exhibited a value of 2.029808 Å, in contrast to the standard's 2.137427 Å. While both values marginally above the optimal threshold (~2.0 Å), 1C-pose1 demonstrates superior spatial accuracy, suggesting a more reliable and stable conformation inside the active pocket.
Significant disparities emerge when evaluating energy components. The E_conf value for 1C-pose1 is –5.78414, signifying little internal strain, whereas the standard has a significantly negative value of –93.9605, indicative of a more energetically favorable

conformation. For E_place, the 1C score is –11.7547, whereas the standard value is –102.304, indicating that the standard exhibits a stronger fit inside the binding pocket. Additionally, the refined scores—E_score1 and E_refine—for 1C are –9.434 and –32.5248, while the standard scores are –11.9107 and –36.5557, respectively. These figures suggest that the standard ligand achieved more effective positioning and subsequent refinement inside the protein's active region, enhancing its binding affinity.

The examination of interactions uncovers an additional dimension of comparison. Compound 1C engages with the protein via two π–H interactions, involving THR 347 (CG2) and PHE 404 (CD1), with interaction distances of 4.37 Å and 4.05 Å and energies of –0.7 and –0.8 kcal/mol, respectively. These interactions, while significant, are rather weak and non-directional in comparison to hydrogen bonds. Conversely, the standard ligand establishes a singular but much stronger hydrogen bond with GLU 353 (OE1) at a proximity of 2.53 Å and an energy of –3.8 kcal/mol, which substantially enhances its stability and binding affinity.

In conclusion, although 1C-pose1 exhibits competitive binding with acceptable energy values and pose stability, it is somewhat less effective than the conventional ligand, particularly with total energy scores and interaction strength. The π–H bonds in 1C are weaker than the robust hydrogen bonding shown by the standard. Nonetheless, the minor variations in affinity and RMSD suggest that compound 1C may still function as a viable lead, particularly if chemically altered to augment polar interactions, including hydrogen bonding.

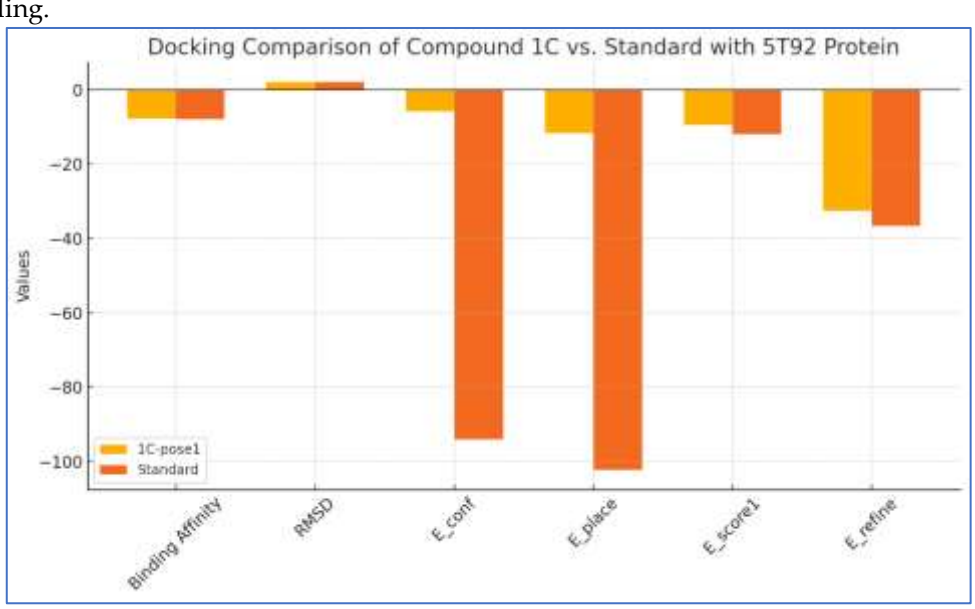

The bar chart compares the docking performance of compound 1C (pose 1) and the standard ligand against the 5T92 protein based on several key parameters: binding affinity, RMSD, E_conf, E_place, E_score1, and E_refine. Lower (more negative) values indicate stronger binding and better energetic stability, while lower RMSD values signify more stable and accurate docking poses. From the chart, the standard ligand performs better in most energy terms (especially E_conf and E_place), indicating a more stable and energetically favorable binding. However, compound 1C still shows competitive results, particularly in RMSD and E_refine, suggesting it adopts a reasonably stable pose and could be a potential candidate for further optimization.

4. Conclusion

The synthesized chalcone derivatives demonstrated promising biological activities, highlighting their potential as anticancer and antibacterial agents. Specifically, compound 1C exhibited significant cytotoxicity against MCF-7 cells, likely due to its lipophilic properties enhancing cellular uptake and promoting apoptosis. Conversely, derivative 1A showed superior antibacterial activity against the tested bacterial strains, indicating its

effectiveness in fighting microbial infections. These results collectively validate the efficacy of structural modifications in enhancing therapeutic potential, emphasizing the critical role of functional group positioning and electronic properties in determining biological outcomes. Furthermore, spectroscopic analyses provided definitive evidence of chalcone formation, reinforcing the reliability of the synthetic approach utilized. Future work will focus on synthesizing additional chalcone analogs with diversified substitution patterns to systematically evaluate their pharmacokinetic profiles and therapeutic efficacy, thereby facilitating the development of more potent anticancer and antimicrobial agents.

REFERENCES

[1] M. S. Sultan, "Challenges of breast cancer treatment through microbial therapeutic delivery," *Microbial Bioactives,* vol. 6, no. 1, pp. 1-15, 2023.

[2] A. K. Nanayakkara, H. W. Boucher, V. G. Fowler Jr, A. Jezek, K. Outterson, and D. E. Greenberg, "Antibiotic resistance in the patient with cancer: Escalating challenges and paths forward," *CA: a cancer journal for clinicians,* vol. 71, no. 6, pp. 488-504, 2021.

[3] V. B. Kilari and T. Oroszi, "The Misuse of Antibiotics and the Rise of Bacterial Resistance: A Global Concern," *Pharmacology & Pharmacy,* vol. 15, no. 12, pp. 508-523, 2024.

[4] Z. H. Ali, D. Saleem, A. K. Abbas, B. S. Rasool, and M. S. Cheyad, "Synthesis and estimation of the insecticide and antibacterial activities for some new amide derivatives," *Indonesian Journal of Chemistry,* vol. 23, no. 6, pp. 1535-1541, 2023.

[5] D. Ni, Y. Li, Y. Qiu, J. Pu, S. Lu, and J. Zhang, "Combining allosteric and orthosteric drugs to overcome drug resistance," *Trends in pharmacological sciences,* vol. 41, no. 5, pp. 336-348, 2020.

[6] A. A. Jawad, N. R. Jber, B. S. Rasool, and A. K. Abbas, "Tetrazole derivatives and role of tetrazole in medicinal chemistry: An article review," *Al-Nahrain Journal of Science,* vol. 26, no. 1, pp. 1-7, 2023.

[7] O. Obidiro, G. Battogtokh, and E. O. Akala, "Triple negative breast cancer treatment options and limitations: future outlook," *Pharmaceutics,* vol. 15, no. 7, p. 1796, 2023.

[8] R. Chaudhari, V. Patel, and A. Kumar, "Cutting-edge approaches for targeted drug delivery in breast cancer: beyond conventional therapies," *Nanoscale Advances,* 2024.

[9] N. A. Alshaye *et al.*, "Synthesis, DFT, and in silico biological evaluation of chalcone bearing pyrazoline ring against Helicobacter pylori receptors," *Heliyon,* vol. 10, no. 14, 2024.

[10] R. K. Hebasur, V. V. Koppal, D. A. Yaraguppi, N. B. Gummagol, R. Kusanur, and N. R. Patil, "Comprehensive Analysis of a Chalcone Derivative as an Anticancer Agent: Structural, Spectroscopic, DFT-Based Computational, Electrochemical, and Pharmacological Investigations," 2025.

[11] L. Siddiqui, M. B. Hawsawi, G. A. Chotana, and R. S. Z. Saleem, "Bis-Chalcones: Recent Reports of Their Diverse Applications in Biological and Material Sciences," *ACS omega,* vol. 9, no. 41, pp. 42061-42090, 2024.

[12] S. K. Mittapalli *et al.*, "Synthesis, Characterization and Evaluation of Antimicrobial and Antioxidant Activities of Novel Chalcone Scaffolds," *Letters in Drug Design & Discovery,* vol. 21, no. 19, pp. 4792-4812, 2024.

[13] T. T. Mohammed, A. H. Obaid, G. F. Hammeed, and A. K. Abbas, "Modification of Sulfadiazine Antibacterial to Promising Anticancer Schiff Base Derivatives: Synthesis and in Vitro Studies," *The International Science of Health Journal,* vol. 2, no. 3, pp. 01-10, 2024.

[14] A. A. Jawad *et al.*, "Local chemical compounds: synthesis and characterization with antibiotic application," 2024.

[15] A. N. Mahmood, T. T. Mohammed, R. N. Abdulridha, A. H. Obaid, and A. K. Abbas, "Modification of Amoxicillin drug antibacterial to promising anti-breast cancer MCF-7 imine derivatives: Synthesis and in vitro studies," *IAR Journal of Medical Sciences,* vol. 5, pp. 1-6, 2024.

[16] H. Karaca and S. Kazancı, "The metal sensing applications of chalcones: The synthesis, characterization and theoretical calculations," *Journal of Molecular Structure,* vol. 1248, p. 131454, 2022.

[17] J. da Cunha Xavier *et al.*, "Spectroscopic analysis by NMR, FT-Raman, ATR-FTIR, and UV-Vis, evaluation of antimicrobial activity, and in silico studies of chalcones derived from 2-hydroxyacetophenone," *Journal of Molecular Structure,* vol. 1241, p. 130647, 2021.

[18] M. C. Romeu *et al.*, "Synthesis, crystal structure, ATR-FTIR, FT-Raman and UV spectra, structural and spectroscopic analysis of (3E)-4-[4-(dimethylamine) phenyl] but-3-en-2-one," *Journal of Molecular Structure,* vol. 1264, p. 133222, 2022.

[19] L. W. Wijayanti, R. T. Swasono, W. Lee, and J. Jumina, "Synthesis and evaluation of chalcone derivatives as novel sunscreen agent," *Molecules,* vol. 26, no. 9, p. 2698, 2021.
[20] A. Wilhelm *et al.*, "Synthesis, characterization and cytotoxic evaluation of chalcone derivatives," *Journal of Molecular Structure,* vol. 1251, p. 132001, 2022.
[21] E. N. Okolo *et al.*, "New chalcone derivatives as potential antimicrobial and antioxidant agent," *Scientific reports,* vol. 11, no. 1, p. 21781, 2021.
[22] R. Rajasagaran *et al.*, "Structural and Optical Characterization of Anthracene and Bis-Anthracene Chalcone Derivatives as Photosensitizers for Dye-Sensitized Solar Cells," *Journal of Molecular Structure,* p. 142694, 2025.
[23] B. Ngameni *et al.*, "Design, synthesis, characterization, and anticancer activity of a novel series of O-substituted chalcone derivatives," *Bioorganic & Medicinal Chemistry Letters,* vol. 35, p. 127827, 2021.
[24] H. Şenol, M. Ghaffari-Moghaddam, G. Ö. A. Toraman, and U. Güller, "Novel chalcone derivatives of ursolic acid as acetylcholinesterase inhibitors: Synthesis, characterization, biological activity, ADME prediction, molecular docking and molecular dynamics studies," *Journal of Molecular Structure,* vol. 1295, p. 136804, 2024.
[25] M. G. Balamon, E. A. El-Bordany, N. F. Mahmoud, A. A. Hamed, and A. E. Swilem, "Exploring the Antioxidant Potency of New Naphthalene-Based Chalcone Derivatives: Design, Synthesis, Antioxidant Evaluation, Docking Study, DFT Calculations," *Chemistry & Biodiversity,* vol. 20, no. 12, p. e202301344, 2023.
[26] S. Priya, M. M. Islam, S. Kasana, B. D. Kurmi, G. D. Gupta, and P. Patel, "Therapeutic potential of chalcone-1, 2, 3-triazole hybrids as anti-tumour agents: a systematic review and SAR studies," *Future Medicinal Chemistry,* pp. 1-17, 2025.
[27] T. A. Santos *et al.*, "Methoxy chalcone derivatives: promising antimicrobial agents against Phytopathogens," *Chemistry & Biodiversity,* vol. 21, no. 11, p. e202400945, 2024.
[28] H. Mirzaei and S. Emami, "Recent advances of cytotoxic chalconoids targeting tubulin polymerization: Synthesis and biological activity," *European journal of medicinal chemistry,* vol. 121, pp. 610-639, 2016.
[29] M. Zhu *et al.*, "Design, synthesis, and evaluation of chalcone analogues incorporate α, β-Unsaturated ketone functionality as anti-lung cancer agents via evoking ROS to induce pyroptosis," *European Journal of Medicinal Chemistry,* vol. 157, pp. 1395-1405, 2018.
[30] H. Shi, Y. Zhou, E. Jia, M. Pan, Y. Bai, and Q. Ge, "Bias in RNA-seq library preparation: current challenges and solutions," *BioMed research international,* vol. 2021, no. 1, p. 6647597, 2021.
[31] V. H. Masand *et al.*, "Estrogen receptor alpha binders for hormone-dependent forms of breast cancer: e-QSAR and molecular docking supported by X-ray resolved structures," *ACS omega,* vol. 9, no. 14, pp. 16759-16774, 2024.
[32] N. Kumar *et al.*, "Most recent strategies targeting estrogen receptor alpha for the treatment of breast cancer," *Molecular Diversity,* vol. 25, pp. 603-624, 2021.